Lattice dynamics of CoO from first principles

U. D. Wdowik* and K. Parlinski
Institute of Technology, Pedagogical University, PL-30-084 Cracow, ul. Podchorazych 2, Poland
(Received 29 December 2006; published 27 March 2007)

Cobaltous oxide (CoO) has been studied by using density-functional theory and the generalized-gradient approximation with correction for Hubbard energy. The calculated electronic structure indicates that CoO is a charge transfer insulator since the Co 3*d* and O 2*p* states are strongly hybridized. The calculated band gap and the spin magnetic moment on divalent Co are in good agreement with the experimentally observed values. The so-called direct method based on calculated Hellmann-Feynman forces is used to obtain the density of states and the dispersion relations of phonons. The temperature dependence of the mean-squared vibrational amplitudes and the behavior of the lattice contribution to heat capacity are analyzed and discussed in the framework of the harmonic approximation. The results of calculations agree with the existing theoretical and experimental data.

DOI: 10.1103/PhysRevB.75.104306 PACS number(s): 63.20.Dj

I. INTRODUCTION

The class of transition-metal oxides is important for modern material science.[1] In particular, they have become more and more interesting for magnetoelectronic applications.[2,3] A variety of electronic, optical, and magnetic properties makes them suitable for the basis of a new type of electronics.[4] Moreover, the physics of transition-metal oxides is very often governed by strong electron correlations, which makes these materials very interesting from the fundamental point of view.

Theoretical investigations employing *ab initio* methods to study the lattice dynamics of strongly correlated electronic systems are a challenging research subject even for simple transition-metal systems (NiO, CoO, FeO, and MnO).[5–7] The difficulties arise mainly from the highly correlated nature of electron interactions (strong on-site Coulomb repulsion between 3*d* electrons), which influence both the electronic structure and lattice dynamics of these oxides.[5]

It is well known that conventional local-density approximations (LDA) or generalized-gradient approximations (GGA) fail to predict the correct ground states, magnetic moments, and magnitude of the energy gaps of strongly correlated electronic systems.[8] The 3*d* transition-metal oxides like MnO, FeO, CoO, and NiO are known to be wide gap Mott-Hubbard or charge transfer antiferromagnetic insulators,[9] while LDA or GGA make them metallic. However, it has been shown that the LDA+U method[10–12] gives the insulating behavior for some correlated systems.[13]

In the LDA+U approach interactions between two correlated states are specified by term U, which is the Coulomb repulsion, and by the local exchange interaction J. In determining the properties of transition-metal oxides the term U is much more important than J, since U is roughly an order of magnitude larger than J. Both U and J parameters can be calculated either self-consistently or by using constrained density-functional calculations;[10] however, such calculations are computationally demanding and may lead to ambiguous results. Moreover, the Hubbard energy U depends on the covalency of the system[14] and it may vary for some element in different polymorphs. Hence the energy U needs to be redefined for each investigated structure. For 3*d* transition-metal oxides J amounts ca. 1 eV (Ref. 10) and the small changes in J do not affect significantly the calculated ground state properties.

The 3*d* transition-metal oxides (NiO, CoO, FeO, and MnO) have the cubic rocksalt structure (space group $Fm\bar{3}m$). Below their respective Néel temperature (T_N) they exhibit antiferromagnetic ordering of type II (AFII),[15] with the magnetic moments on metal ions arranged into ferromagnetic planes of opposite spins being repeated in altering order along the ⟨111⟩ direction. The spin-up and spin-down metal ions constitute two magnetic sublattices, and therefore the magnetic cell is twice as large as the crystallographic unit cell. The onset of magnetic ordering is accompanied by a slight rhombohedral distortion along the ⟨111⟩ direction.[16]

Paramagnetic CoO has the lattice constant of 4.26 Å.[17,18] Its insulating state is characterized by an energy gap of about 2.8 eV,[19] and a total magnetic moment on cobalt ion of about $3.8\mu_B$.[15,20]

The first principle phonon calculations of cobalt oxide, having simple rocksalt-type structure, have been unsuccessful since contributions arising from strong electron correlations have not been taken into account. Such an approach leads to an appearance of unphysical imaginary phonon frequencies. In the present work we include into the interaction potentials the Hubbard energy U and the exchange J terms to better handle the electron correlations. It is shown that, using appropriate U and J, the density-functional theory (DFT) approach combined with the direct method can properly describe the frequencies of the phonon dispersion curves of antiferromagnetic CoO.

II. COMPUTATIONAL DETAILS

The calculations have been performed within the spin-polarized DFT with the Vienna *ab initio* simulation package VASP.[21–23] The exchange-correlation functional in the form of GGA-PW91 was used.[24] The spin interpolation of Vosko *et al.*[25] was applied. The on-site Coulomb repulsion according to the approach of Dudarev *et al.*[12] was taken into account. The Kohn-Sham equations were solved via iterative

matrix diagonalization based on the minimization of the norm of the residual vector to each eigenstate and optimized charge- and spin-mixing routines.[26] The valence electrons of cobalt and oxygen were represented by the configurations $(3d^8 4s^1)$ and $(2s^2 2p^4)$, respectively. The ionic cores were described by the projector augmented wave pseudopotentials.[23,27] The one-electron Kohn-Sham wave functions as well as the charge density were expanded in a plane-wave basis set which contained components with energies up to 520 eV. The rhombohedral supercell containing 64 atoms was sampled using $2\times2\times2$ k-point mesh generated by the Monkhorst-Pack scheme.[28] This corresponds to grid of $32\times32\times32$ for the four-atom primitive cell. Density of states has been calculated with the $6\times6\times6$ k-point mesh and using the linear tetrahedron method with Blöchl corrections.[29] The supercell was optimized with a quasi-Newton algorithm using Hellmann-Feynman forces. The optimization of the ionic positions and the lattice constant continued until the forces acting on each atom were negligible (less than 10^{-5} eV/Å). The rhombohedral angle is very close to the right angle, and therefore in the following calculations the supercell retaining the cubic symmetry is assumed.

The phonon dispersion relations and phonon density of states have been calculated within the harmonic approximation and by the direct method,[30] the latter using forces calculated via Hellmann-Feynman theorem. The forces were generated by displacing four symmetry inequivalent atoms (two Co and two O atoms) with the amplitude of 0.03 Å. Twelve displacements were calculated.

III. RESULTS AND DISCUSSION

A. Structure and magnetization

The proper description of the ground state of CoO requires to take into account the on-site Coulomb repulsion between localized Fe $3d$ electrons. The DFT+U method improves the predictions of the magnitude of magnetic moment and band gap. First, calculations were performed for U ranging from 1 to 9.1 eV, and with $J=1$ eV. They resulted in the energy gap, magnetic moment, and lattice constant dependence as shown in Fig. 1. The lattice constant shows only a weak dependence upon U, in contrast to the energy gap, which is very sensitive to the choice of U. All energies U, which are smaller than 5 eV, considerably underestimate the energy gap. The $U=1$ eV corresponds to the GGA limit at which the energy gap vanishes. The magnetic moment behaves smoothly versus U and changes by ca. 17% throughout the entire U range. Comparing the dependences shown in Fig. 1 with the available experimental data, one finds the values of $U=7.1$ eV and $J=1$ eV as the most appropriate to be used in further detailed calculations. It should be noted that $U=7.8$ eV and $J=0.92$ eV were obtained by Anisimov *et al.*[10]

The crystal geometry optimization was performed with $U=7.1$ eV and $J=1$ eV. It resulted in the rhombohedrally distorted structure of a space group D_{3d}^5 $(R\bar{3}m)$. The calculated lattice constant of 4.27 Å is very close to the experimental lattice parameter of the paramagnetic NaCl structure

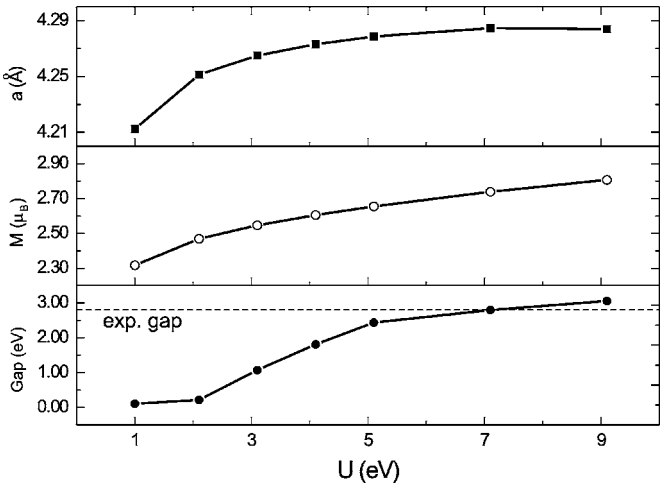

FIG. 1. Lattice constant (a), magnetic moment (M), and the energy gap dependence upon U for GGA+U calculations. The exchange parameter $J=1$ eV. The dashed line represents the experimental value of the energy gap.

(4.26 Å).[17,18,31] The rhombohedral distortion along the ⟨111⟩ direction is as small as 0.3°. This rhombohedral GGA+U solution arises naturally from the AFII symmetry of the rocksalt structure.

The difference in the ground-state energies of rhombohedral and rocksalt structures is very small; albeit the rhombohedral solution is favored.

The calculated magnetic moment of $2.74\mu_B$ follows from the difference in spin-up and spin-down densities. The orbital contribution has not been taken into account. Theoretically predicted spin magnetic moment on cobalt ion in CoO ranges from $2.63\mu_B$ to $2.69\mu_B$.[10,32–34] From the neutron diffraction measurements the total magnetic moment in CoO has been determined as $3.98(6)\mu_B$,[17] $3.8\mu_B$,[15,20] and $3.35\mu_B$.[35] It is well known that the orbital angular momentum of Co^{2+} is only partly quenched by the crystal field. Hence, assuming that spin and orbital moments are collinear,[15] one can estimate the orbital contribution as $1.24\mu_B$. It follows from the total magnetic moment of $3.98\mu_B$. It leads also to an orbital-to-spin angular momentum ratio of $L/S=0.91$. The magnetic x-ray scattering[36] shows that $L/S=0.95$ for CoO.

B. Electronic structure reinvestigation

The GGA+U calculations of the electronic density of states of CoO lead to the energy gap of 2.77 eV for $U=7.1$ eV and $J=1$ eV. It is in agreement with the experimentally determined value of 2.5(3) eV.[19]

The Co^{2+} ion in the high spin state configuration has the $3d$ states split by the exchange interaction into minority- and majority-spin states. When the cobalt ion is located in the octahedral ligand field further splitting into triplet of t_{2g} symmetry and doublet having e_g symmetry occurs. The $3d$ spin-up t_{2g} and e_g orbitals of Co^{2+} are filled, while the $3d$ spin-down t_{2g} state remains only partly occupied. Hence the above-mentioned electronic configuration can be written as follows: $[(t_{2g}\uparrow)^3(e_g\uparrow)^2(t_{2g}\downarrow)^2]$.

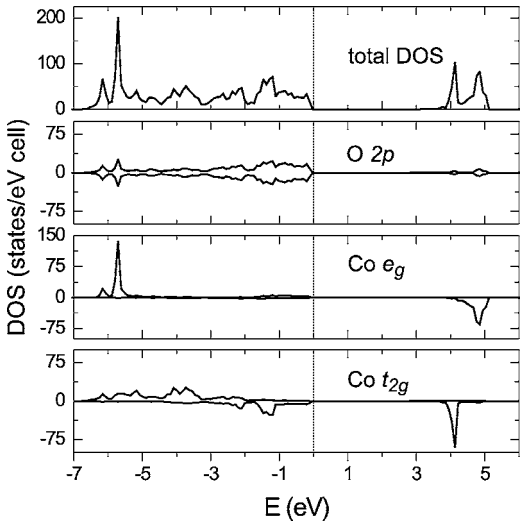

FIG. 2. Total and orbital projected DOS for CoO calculated within GGA+U with U=7.1 eV. The positive (negative) pDOS represent the spin-up (spin-down) component of e_g and t_{2g} projections, respectively. The top of the valence band is taken as the reference energy.

The total, spin-polarized, and orbital projected densities of states are shown in Fig. 2. The significant admixture of the oxygen 2p states at the top of the valence band seems to be in qualitative agreement with the optical absorption experiments,[37] which indicate the hybridization of Co 3d and O 2p orbitals. The mixed O 2p-Co 3d states play an important role in the characterization of the insulating nature of CoO. It can be seen in Fig. 2 that the highest occupied valence bands are dominated by oxygen 2p states, which are hybridized with Co t_{2g} minority spin states. The O 2p and Co $t_{2g}\downarrow$ partial waves have nearly the same spectral weight at the top of the valence band. Figure 2 shows that the lowest unoccupied conduction states result from the narrow band being mainly due to Co t_{2g} spin-down component, and that t_{2g} state has much higher spectral weight than the e_g orbital. The separation between e_g minority and majority spin states amounts to ca. 10 eV, while the peak distance between unoccupied $e_g\downarrow$ and $t_{2g}\downarrow$ states is less than 1 eV. The exchange splitting of about 1 eV can also be seen from the t_{2g} density of states.

IV. LATTICE DYNAMICS

The results of lattice dynamics calculations for CoO are shown in Fig. 3. The phonon dispersion relations along high-symmetry points of the Brillouin zone are compared with the inelastic neutron scattering measurements performed at 110 K by Sakurai *et al.*[38] Our calculations reproduce the experimentally determined phonon dispersion curves quite well. Only a small discrepancies for transverse optic (TO) frequencies along Γ-L direction is observed. The lowest phonon branches belong to the transverse acoustic (TA) modes reaching frequencies of about 5 THz at the Brillouin zone boundary. The dispersion relations of the TA branches are practically monotonous, except for the visible flattening while approaching the zone boundaries.

Since CoO can be regarded as a wide-gap insulator, calculations of the phonon frequencies at the Γ point require taking into account the coupling between atomic displacements and the long-range macroscopic electric field. This field splits the infrared-active optical modes (IR) to transverse (TO) and longitudinal (LO) components. It is the so-called LO-TO splitting. Generally, the IR internal vibrations have TO and LO modes absorbing at different frequencies, and the LO frequency (ω_{LO}) is greater than the TO frequency (ω_{TO}) because the local electric field causes polarization of the surrounding atoms in the opposite direction for the LO mode, but in the same direction for the TO mode. TO phonon frequencies are calculated within the direct method, but the LO modes require the introduction of the nonanalytical term into the dynamical matrix.[39] This term generally depends upon the Born effective charge tensor and the high-frequency dielectric constant ϵ_∞. In the present work the Born effective charges for cobalt and oxygen, $|Z^*|$, have been estimated using the $q\rightarrow 0$ limit technique and the Lyddane-Sachs-Teller relation $\omega_{\mathrm{LO}}^2-\omega_{\mathrm{TO}}^2\sim|Z^*|^2/\epsilon_\infty$. For our calculated ω_{TO} =10.25 THz and the experimentally determined ω_{LO} =15.75 THz, and ϵ_∞=5.3,[31] $|Z^*|$ equals 2.06.

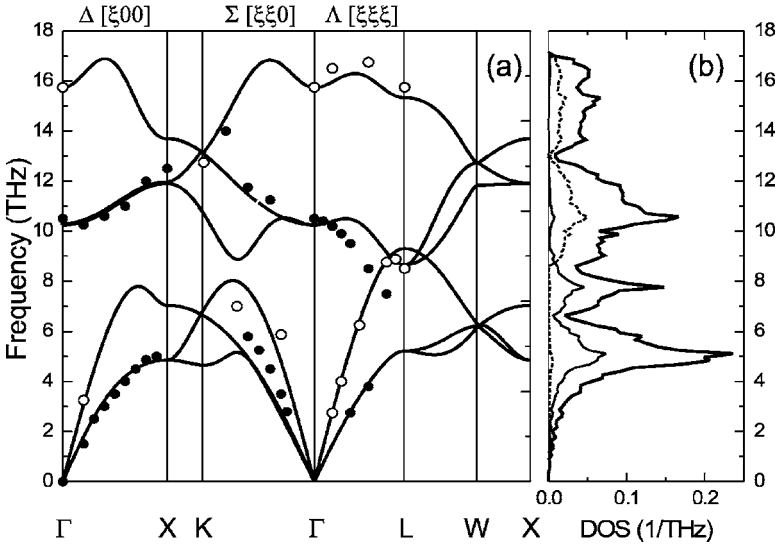

FIG. 3. (a) Phonon dispersion curves and (b) phonon density of states for CoO obtained from our *ab initio* calculation (solid line) and from inelastic neutron scattering experiments (Ref. 38) at 110 K (dots). Solid and open symbols indicate transverse and longitudinal modes, respectively. The high-symmetry points are labeled according to FCC Brillouin zone. The thick solid line in (b) represents the total DOS while the thin and dashed lines are due to Co and O partial densities of states.

TABLE I. Γ-point optical frequencies (ω_{TO}, ω_{LO}), static dielectric constants ($\epsilon_\infty, \epsilon_0$), and Born effective charges ($|Z^*|$) for CoO.

	Present work	Neutron scattering (Ref. 38)	Infrared spectroscopy (Ref. 31)
ω_{TO} (THz)	10.25	10.50	10.40–16.49
ω_{LO} (THz)	15.73	15.75	16.30–16.40
ϵ_∞			5.3
ϵ_0			12.9
$\|Z^*\|$	2.06	2.06	1.78

The calculated frequency of the infrared-active mode (T_{1u}) $\omega_{TO}=10.25$ THz is close to those measured either by neutron scattering [10.50 THz (Ref. 38)] or by infrared-absorption spectroscopy [10.40–10.49 THz (Ref. 31)]. A comparison between theoretical and the available experimental data is shown in Table I.

Compared to the prediction of earlier rigid-ion model,[38] our first principles calculations show better agreement for the LO branch in the [ξξξ] direction, while the TO branch for the same direction is slightly overestimated. All the calculated branches in the [00ξ] direction reproduce the neutron scattering data quite well, and only the small discrepancy for acoustic phonons in the [ξξ0] direction is observed.

Figure 3(b) shows total and partial density of phonon states. One can see that the main contribution to acoustic phonons comes from the cobalt sublattice, while the high frequency phonons are dominated by the dynamics of the light oxygen ions.

Additionally, the elastic constants C_{11}, C_{12}, and C_{44} were calculated from the linear stress-strain relations. Results are shown in Table II. The best agreement between DFT-based and rigid-ion model calculations[38] is observed for C_{44}, while the largest deviation (ca. 19%) is encountered for C_{12}. Theoretical C_{ij} stay in close agreement with the experiment.[40]

The phonon contribution to the thermodynamical properties could be calculated from the phonon density of states. The contribution from lattice vibrations to the total heat capacity of CoO is shown in Fig. 4. Within the harmonic approximation the difference between the heat capacity at constant pressure, C_p, and the heat capacity at the constant volume, C_v, is given by $C_p - C_v = TV\beta^2 B$, where β is the thermal expansion coefficient, V indicates volume, T stands for temperature, and B is the isothermal bulk modulus. The thermal expansion coefficient of 4×10^{-5} K^{-1} could be estimated from data cited in Ref. 42. The remaining quantities

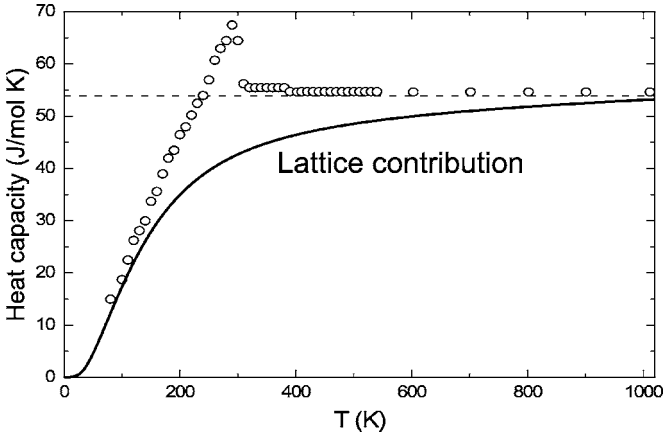

FIG. 4. Calculated and experimental specific heat for CoO. Experimental data (open points) are taken from Ref. 41. The solid curve and dashed line indicate lattice contribution and the Dulong-Petit law, respectively.

were derived from our *ab initio* calculations. The temperature range is limited to 1000 K to avoid influence of anharmonicity. The maximal difference between C_p and C_v is 4 J/(mol K) at high temperatures. The measured heat capacity may contain variety of contributions depending upon the nature of the material studied. In the case of CoO, the heat capacity can be considered to be a sum of at least three components, i.e., the lattice term, the magnetic term, and the electronic (Schottky) term. The lattice contribution shown in Fig. 4 follows the Debye model and approaches the Dulong-Petit limit at high temperatures. Additionally, the background contribution from the disorder of magnetic moments can be observed. CoO undergoes the magnetic transition at 290 K, and therefore a λ-type behavior in the vicinity of the Néel temperature can be seen as well.

One can use the calculated density of states to obtain the mean-squared displacements of ions as a function of temperature. The form factor which describes the diffraction scattering contains the Debye-Waller factor defined as

$$\exp\{-W_\mu(\mathbf{k})\}, \tag{1}$$

where

$$W_\mu(\mathbf{k}) = \frac{1}{2}(2\pi\mathbf{k})\cdot\mathbf{B}(\mu)\cdot(2\pi\mathbf{k}). \tag{2}$$

$\mathbf{B}(\mu)$ is a 3×3 matrix. It represents the static correlation function of displacements $U(\mu)$ of atom μ from the equilibrium positions. Elements of matrix $\mathbf{B}(\mu)$ are the following:

TABLE II. Experimental and calculated elastic constants (C_{ij}), bulk (B), and shear (μ) moduli for CoO crystal. All data are expressed in GPa. Values in brackets are for 425 K and the remaining data were taken at 110 K.

Results	C_{11}	C_{12}	C_{44}	B	μ
From stress-strain	256	148	91	184	54
Ref. 38	307 (277)	183 (180)	90 (91)	224 (212)	62 (49)
Ref. 40	261	145	83	184	58

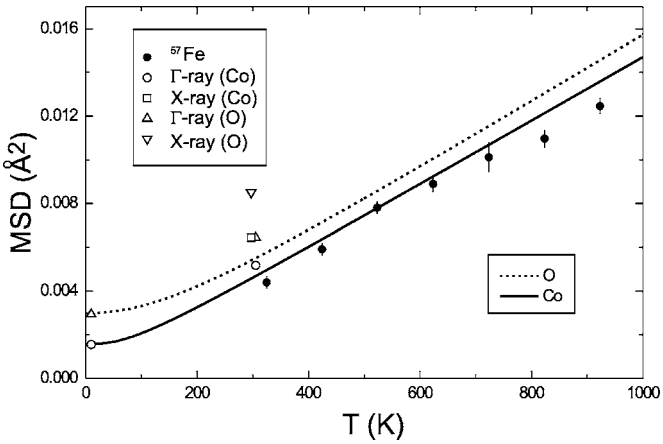

FIG. 5. Mean-squared displacements (MSD) vs temperature for cations and anions in CoO. Solid and dashed curves represent cobalt and oxygen contributions, respectively. Solid symbols are due to ^{57}Fe substitutional impurity in CoO host matrix (Ref. 44). The Γ-ray data (Ref. 18) are shown as open circles (Co) and up-triangles (O). X-ray experiments (Ref. 43) are denoted by open square (Co) and down-triangle (O).

$$B_{ij} = \langle U_i(\mu) U_j(\mu) \rangle. \tag{3}$$

The matrix $\mathbf{B}(\mu)$ is symmetric and represents the mean-squared displacements of atom μ. It is expressed by the off-diagonal partial density of states $g_{il,\mu}(\omega)$ in the following way:[30]

$$B_{il}(\mu) = \frac{\hbar r}{2M_\mu} \int_0^\infty d\omega \, g_{il,\mu}(\omega) \omega^{-1} \coth\left(\frac{\hbar\omega}{2k_B T}\right), \tag{4}$$

where $\hbar$ is the Planck constant, k_B is the Boltzmann constant, and T is the temperature. M_μ and r denote mass of the atom μ and the number of degrees of freedom in the unit cell, respectively.

The mean-squared displacements versus temperature for cations and anions are plotted in Fig. 5 and compared to those determined from Γ-ray,[18] x-ray,[43] and Mössbauer spectroscopy[44] experiments. Room temperature mean-squared displacements measured by x-ray scattering are significantly higher than those obtained from Γ-ray experiment. It is suggested that either the lack of thermal diffusive scattering correction or the monochromator used are responsible for such an effect.[18] However, at low temperature (10 K) the Γ-ray data stay in very good agreement with the present calculations. The difference between experimental and theoretical results is much more pronounced for oxygens and at elevated temperatures. Contrary to the Γ-ray results no anisotropy in zero-point vibration neither for Co nor for O is observed.

Emission Mössbauer spectroscopy was used to study vibrational properties of diluted ^{57}Fe impurity in the host CoO matrix.[44] The daughter iron being a product of the radioactive decay of parent ^{57}Co reflects the local vibrational properties of the host matrix, at least on the Mössbauer spectroscopy time scale (141 ns). Hence, the results of our calculations are close to mean-squared displacements determined by Mössbauer effect. It should be mentioned that the isotope effect is insignificant here and can be neglected. One can see in Fig. 5 that the slopes for cobalts and irons are practically the same.

Mean-squared amplitudes of vibrations were used to evaluate the Debye temperature (Θ_D) of CoO. The calculated Θ_D equals 596 K as compared to 440(11) K, the latter being obtained from Mössbauer spectroscopy studies.[44]

V. CONCLUSIONS

The calculated electronic structure indicates that CoO is a charge-transfer insulator rather than Mott-Hubbard insulator. The energy gap and magnetic moments on cobalt ions agree with the experimental values. Calculated elastic constants, mean-squared displacements of ions, and the lattice contribution to heat capacity at elevated temperatures reproduce the experimental data quite well.

The on-site Coulomb interactions between *3d* electrons, represented by Hubbard energy U, is crucial for the proper description of the band structure and the lattice dynamics. Calculations carried out with too low U_{eff} ($U_{\text{eff}}=U-J$), e.g., $U_{\text{eff}}=3$ eV, will result in the underestimation of either the energy gap or spin magnetic moment on Co ion. We found that the Hubbard term determines to a large extent calculated phonon densities of states and the phonon dispersion curves of CoO. The lower U_{eff}, the more apparent underestimation of both LO and TO frequencies is seen. Small U_{eff} implies too low repulsion in the *3d* electron shell. Indeed, when the charge is allowed to flow into the *3d* shell, an unphysical mode softening of phonon branches is observed. The charge transfer takes place between nearest-neighbor ions and therefore it influences predominantly the longitudinal optical mode. The acoustic branches are somewhat better predicted if the lower U_{eff} is applied. However, it should be pointed out that the calculations of lattice mode frequencies for $U_{\text{eff}}<2$ eV lead to negative frequencies of acoustic modes due to the instability of CoO structure. Such artificial soft modes arise from the underestimated values of the Hellmann-Feynman forces.

ACKNOWLEDGMENTS

This work was supported by the Polish Ministry of Scientific Research (MNiI), Grant No. 3T11F 031 29. Interdisciplinary Modeling Center (ICM), Warsaw University, Poland is acknowledged for providing the computer facilities under Grant No. G28-12.

*Corresponding author. FAX: +48126372243. Email address: sfwdowik@cyf-kr.edu.pl

[1] Y. A. Soh and G. Aeppli, Nature (London) **417**, 392 (2002).
[2] S. Jin, Th. Tiefel, M. McCormarck, R. Fastnacht, and R. Rchen, Science **264**, 413 (1994).
[3] A. J. Mills, Nature (London) **392**, 147 (1998).
[4] T. Tokura, Phys. Today **56**, 50 (2003).
[5] S. Y. Savrasov and G. Kotliar, Phys. Rev. Lett. **90**, 056401 (2003).
[6] S. L. Dudarev, L. M. Peng, S. Y. Savrasov, and J. M. Zuo, Phys. Rev. B **61**, 2506 (2000).
[7] S. Massidda, M. Posternak, A. Baldereschi, and R. Resta, Phys. Rev. Lett. **82**, 430 (1999).
[8] K. Terakura, T. Oguchi, A. R. Williams, and J. K. Kübler, Phys. Rev. B **30**, 4734 (1984); T. Oguchi, K. Terakura, and A. R. Williams, *ibid.* **28**, 6443 (1983); P. Dufek, P. Blaha, V. Sliwko, and K. Schwarz, *ibid.* **49**, 10170 (1994).
[9] G. A. Sawatzky and J. W. Allen, Phys. Rev. Lett. **53**, 2339 (1984); J. Zaanen, G. A. Sawatzky, and J. W. Allen, *ibid.* **55**, 418 (1985).
[10] V. I. Anisimov, J. Zaanen, and O. K. Andersen, Phys. Rev. B **44**, 943 (1991).
[11] V. I. Anisimov, I. V. Solovyev, M. A. Korotin, M. T. Czyżyk, and G. A. Sawatzky, Phys. Rev. B **48**, 16929 (1993).
[12] S. L. Dudarev, G. A. Botton, S. Y. Savrasov, C. J. Humphreys, and A. P. Sutton, Phys. Rev. B **57**, 1505 (1998).
[13] I. I. Mazin and V. I. Anisimov, Phys. Rev. B **55**, 12822 (1997).
[14] M. S. Hybertsen, M. Schlüter, and N. E. Christensen, Phys. Rev. B **39**, 9028 (1989).
[15] W. L. Roth, Phys. Rev. **110**, 1333 (1958).
[16] B. Morosin, Phys. Rev. B **1**, 236 (1970); B. T. M. Willis and H. P. Rooksby, Acta Crystallogr. **6**, 827 (1953); L. C. Bartel and B. Morosin, Phys. Rev. B **3**, 1039 (1971).
[17] W. Jauch, M. Reehuis, H. J. Bleif, F. Kubanek, and P. Pattison, Phys. Rev. B **64**, 052102 (2001).
[18] W. Jauch and M. Reehuis, Phys. Rev. B **65**, 125111 (2002).
[19] J. van Elp, J. L. Wieland, H. Eskes, P. Kuiper, G. A. Sawatzky, F. M. F. de Groot, and T. S. Turner, Phys. Rev. B **44**, 6090 (1991).
[20] D. Herrmann-Ronzaud, P. Burlet, and J. Rossat-Mignod, J. Phys. C **11**, 2123 (1978).
[21] G. Kresse and J. Hafner, Phys. Rev. B **47**, 558 (1993); **49**, 14251 (1994).
[22] G. Kresse and J. Furthmüller, Phys. Rev. B **54**, 11169 (1996); Comput. Mater. Sci. **6**, 15 (1996).
[23] G. Kresse and D. Joubert, Phys. Rev. B **59**, 1758 (1999).
[24] J. P. Perdew, J. A. Chevary, S. H. Vosko, K. A. Jackson, M. R. Pederson, D. J. Singh, and C. Fiolhais, Phys. Rev. B **46**, 6671 (1992).
[25] S. H. Vosko, L. Wilk, and M. Nusair, Can. J. Phys. **58**, 1200 (1980).
[26] P. Pulay, Chem. Phys. Lett. **73**, 393 (1980); D. M. Wood and A. Zunger, J. Phys. A **18**, 1343 (1985); D. D. Johnson, Phys. Rev. B **38**, 12807 (1988).
[27] P. E. Blöchl, Phys. Rev. B **50**, 17953 (1994).
[28] H. J. Monkhorst and J. D. Pack, Phys. Rev. B **13**, 5188 (1976).
[29] P. E. Blöchl, O. Jepsen, and O. K. Andersen, Phys. Rev. B **49**, 16223 (1994).
[30] K. Parlinski, Z-.Q. Li, and Y. Kawazoe, Phys. Rev. Lett. **78**, 4063 (1997); K. Parlinski, Software Phonon, Cracow, 2005.
[31] P. J. Gielisse, J. N. Plendl, L. C. Mansur, R. Marshall, S. S. Mitra, R. Mikolajewicz, and A. Smakula, J. Appl. Phys. **36**, 2446 (1965).
[32] Pan Wei and Z. Q. Qi, Phys. Rev. B **49**, 10864 (1994).
[33] I. V. Solovyev, A. I. Liechtenstein, and K. Terakura, Phys. Rev. Lett. **80**, 5758 (1998).
[34] X. B. Feng, Phys. Rev. B **69**, 155107 (2004).
[35] S. Hufner and G. K. Wertheim, Phys. Rev. B **7**, 5086 (1973).
[36] W. Neubeck, C. Vettier, F. de Bergevin, F. Yakhou, D. Mannix, L. Ranno, and T. Chatterji, J. Phys. Chem. Solids **62**, 2173 (2001).
[37] J. P. Kemp, S. T. P. Davies, and P. A. Cox, J. Phys.: Condens. Matter **1**, 5313 (1989); A. Gorschlüter and H. Merz, Phys. Rev. B **49**, 17293 (1994).
[38] J. Sakurai, W. J. L. Buyers, R. A. Cowley, and G. Dolling, Phys. Rev. **167**, 510 (1968).
[39] R. M. Pick, M. H. Cohen, and R. M. Martin, Phys. Rev. B **1**, 910 (1970).
[40] C. N. R. Rao and G. V. Subba Rao, Report No. NSRDS-NBS, 1974 (unpublished), Vol. 49, p. 140.
[41] E. G. King and A. U. Christensen, *U. S. Bur. Mines Tech. Paper* 80, 1800 (1956); E. G. King, *U. S. Bur. Mines Tech. Paper* 80, 2399 (1956); E. N. Abarra, K. Takano, F. Hellman, and A. E. Berkowitz, Phys. Rev. Lett. **77**, 3451 (1996).
[42] C. Massobrio and M. Meyer, J. Phys.: Condens. Matter **3**, 279 (1991).
[43] S. Sasaki, F. Fujino, and Y. Takeuchi, Proc. Jpn. Acad., Ser. B: Phys. Biol. Sci. **55**, 43 (1979).
[44] K. Ruebenbauer and U. D. Wdowik, J. Phys. Chem. Solids **65**, 1785 (2004).